Available online at www.sciencedirect.com

ScienceDirect

Procedia CIRP 101 (2021) 126–129

www.elsevier.com/locate/procedia

9th CIRP Conference on High Performance Cutting (HPC 2020)

Surface error shape identification for 3-axis milling operations

Lorenzo Morelli[a], Niccolò Grossi[a,*], Antonio Scippa[a], Gianni Campatelli[a]

[a]*Department of Industrial Engineering, University of Firenze, Via di Santa Marta 3, 50139, Firenze, Italy*

* Corresponding author. Tel.: +39- 055-2758726; *E-mail address:* niccolo.grossi@unifi.it

Abstract

In 3-axis milling operations the surface error caused by the tool/workpiece static deflection assumes a certain shape along the axial depth of cut. The error shape changes considerably according to the cutting strategy, tool geometry and cutting parameters. This paper presents a comprehensive method to identify all the types of surface error profile in down-milling, proposing dedicated analytical equations. This approach has been experimentally validated to assess its accuracy and limits. The results of this approach are meant to ease the surface error prediction and measurement by reducing the number of points to consider along the axial depth of cut.

Keywords: End milling; Surface analysis; Tool geometry; Stiffness.

1. Introduction

In 3-axis milling operations, the prediction of surface errors [1] represents the core of many approaches [2-4] aiming at achieving the required tolerance on a machined component at minor costs and higher productivity. Most of the prediction approaches evaluate numerically the surface error along the axial depth of cut considering both static [5] and dynamic aspects [6]. However, information about the axial shape of the surface error remain unused limiting the effectiveness of the prediction techniques. Indeed, the surface error shape, caused by the tool static deflection is characterized by key points whose axial positions change according to tool geometry, cutting parameters and cutting strategy., since it is affected by the cutting forces acting on the surface when it is generated (i.e., surface generating force). Won-Soo Yun et al.[7] tested limited cutting condtions and estimated the axial position of one key point using the angular position of the cutting force's peak value simulated with a mechanistic approach. Although the study proved the relationship between cutting force and the axial position of a key point, very few types of surface error shapes were analyzed. M. N. Islam et al.[8] tested operations with high axial depths of cut cutting and identified four key points whose axial positions were analytically validated. Nonetheless the increased number of expressions obtained only one type of surface error shape was considered. Starting from the force shape classification made by Yang. L et al.[9], Desai et al.[10] showed various types of surface error shapes in down milling depending on the cutting parameters and tool geometry. Each shape is characterized by a certain number of key points whose axial positions were expressed analytically and experimentally validated. Despite this, not all the types of surface error shapes were identified. This paper, starting from the results by Yang. L et al.[9] extends the classification of cutting force shapes in down milling, including the effect of helix angle and different cutting edges involved (i.e., overlap). From this classification, following the same approach by Desai et al.[10], all the types of surface generating force shape are identified and the analytical equations of the key points axial positios, for all the corresponding types of surface error shape, are presented. The effectiveness of such equations was proved by the proposed validation procedure.

10.1016/j.procir.2021.02.016

2. Proposed Approach

In 3-axis milling operations, the definitive machined surface is produced at the time when the cutting edge is perpendicular to the workpiece. Depending on the cutting strategy adopted, this condition occurs at the cutter exit angle, φ_{out}, (down milling Fig. 1a) or at the cutter entry angle, φ_{in}, (up milling). Nonetheless, in both strategies, as the tool rotates, due to the helix angle of the cutter, the instant, which the machined surface is generated, changes continuously along the axial depth of cut therefore the machined surface as a whole is not generated in a single moment but step by step at different instants. This mechanism ensures that, for each instant that a portion of the machined surface is generated, the corresponding surface error depends on the resultant cutting force acting on the tool, in the direction normal to the surface (F_y) at the exact same instant. For this reason, to characterize and classify the shape of the surface error, first the shape of (F_y), as a function of the engagement angle (ϑ), must be examined.

2.1 Single fluted endmill force classification in down-milling

In peripheral milling, for a single fluted endmill, the shape of the cutting force depends on both the cutter engagement angle (α_{en}) and the cutter swept angle (α_{sw}). These angles are related to the cutting parameters thanks to the following equations:

$$\alpha_{en} = (\varphi_{out} - \varphi_{in}) = \text{acos}\left(1 - {}^{2ar}/_{D}\right) \quad (1)$$

$$\alpha_{sw} = k_b ap \quad ; \quad k_b = {}^{2tan(\alpha_{el})}/_{D} \quad (2); (3)$$

where ar is the radial depth of cut, ap is the axial depth of cut, D is the tool's diameter and α_{el} is the cutter's helix angle parameters. As it is reported by Yang. L et al[9], three shape of cutting force are distinguished (Fig. 1b) by comparing ap and ar with two other parameters, the critical axial depth of cut (apc) and the critical radial depth of cut (arc):

- Type I: $ar < ar_c$ and $ap < ap_c$
- Type II: $ar < ar_c$ and $ap \geq ap_c$
- Type III: $ar \geq ar_c$

where ap_c represents the axial depth of cut which allows α_{sw} to be equal to α_{en} and it can be easily obtained by combining equation (1) and (2). On the other hand, ar_c is defined as the radial depth of cut which allows to reach the maximum F_y, found in the full-immersion (i.e., slotting) condition. This parameter, for down milling operations, is obtained with the following equation:

$$ar_c = {}^{D}/_{2}\,(1 - \cos(\alpha_{sw} + \varphi_{out} - \varphi_{max})) \quad (4)$$

where φ_{max} is the angular position of the peak value of F_y in a slotting condition. This value (φ_{max}) cannot be easily foreseen, however, considering a mechanistic cutting force model (5), like the one used by Grossi et al [4], an analytical expression (6) for φ_{max} was elaborated.

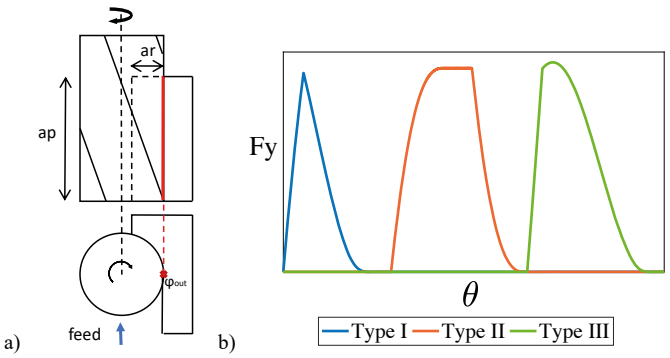

Fig. 1. (a) down-milling cutting scheme; (b) force profiles

$$F_t = K_{tc} h \;\; ; F_r = K_{rc} h \; ; \; h = fz \cdot \sin(\vartheta) \quad (5)$$

where K_{tc} and K_{rc} are respectively the tangential and radial cutting coefficients while h represents the chip thickness and fz is the feed per tooth.

$$\varphi_{max} = \pi + {}^{\alpha_{sw}}/_{2} - \frac{\sqrt{K_{tc}^2 + K_{rc}^2} + K_{tc}}{K_{rc}} \quad (6)$$

The equation (6) allows to identify the Type III F_y shape, and it differs from the one by Yang. L et al [9] that refers to the resultant cutting force along in the direction normal to the surface.

2.2. Multiple fluted endmill force classification in down-milling

To fully identify cutting force shapes, the effect of multiple flutes should be included as the sum of the single flute F_y shapes involved in the cutting operation. Therefore, the classification of the cutting forces profiles for a multi flute endmill is achieved by analysing, for each one of three types mentioned in the previous section, how single F_y shapes may overlap one another. Yang. L et al [9] depending on the engagement angles (α_{en}, α_{sw}) and tool's pitch angle (φ_z), classified the amount of overlap between two single flute F_y shapes, limiting the overlap to two flutes. This distinction does not consider how the features of each single flute F_y shape may affect the amount of overlap, moreover, the number of single flute F_y shapes involved in the cut, depending on the cutting parameters and tool geometry, may not be limited to two only. For this reason, in this work, an extended classification, to evaluate the amount of overlap considering both the features of each single flute F_y shape and the number of flutes involved in the cut (n), has been proposed. This new classification defines the degrees of overlap with letters as Yang. L et al [9],and it uses L for low overlap, M for medium overlap and H for high overlap. Moreover, two novel categories are added, m and h which represent two cases of medium and high overlap that are possible only for type II single flute F_y shape. Table 1 summerizes the degrees of overlap between the first single flute F_y shape and the i-th following single flute F_y shape involved in the cut (i=1, 2, ..., n-1) adopting α_{en}, α_{sw}, the tool's pitch angle (φ_z) and α_{enc} ($\alpha_{enc} = \alpha_{sw} + \varphi_{out} - \varphi_{max}$).

Table 1. Overlap classification.

	Type I	Type II	Type III
L	$\alpha_{en}+\alpha_{sw} \geq i\varphi_z$ $\alpha_{en} < i\varphi_z$	$\alpha_{en}+\alpha_{sw} \geq i\varphi_z$ $\alpha_{sw} < i\varphi_z$	$\alpha_{enc} < i\varphi_z$ $\alpha_{sw}+(\alpha_{en}-\alpha_{enc}) < i\varphi_z$
M	$\alpha_{en} \geq i\varphi_z$ $\alpha_{sw} < i\varphi_z$	$\alpha_{sw} < i\varphi_z+\alpha_{en}$ $\alpha_{en} < i\varphi_z$; $\alpha_{sw} \geq i\varphi_z$	$\alpha_{enc} \geq i\varphi_z$ $\alpha_{sw}+(\alpha_{en}-\alpha_{enc}) < i\varphi_z$
H	$\alpha_{en} \geq i\varphi_z$ $\alpha_{sw} \geq i\varphi_z$	$\alpha_{sw} < i\varphi_z+\alpha_{en}$ $\alpha_{en} \geq i\varphi_z$; $\alpha_{sw} \geq i\varphi_z$	$\alpha_{enc} \geq i\varphi_z$ $\alpha_{sw}+(\alpha_{en}-\alpha_{enc}) \geq i\varphi_z$
m	*n/a*	$\alpha_{sw} \geq i\varphi_z+\alpha_{en}$ $\alpha_{en} < i\varphi_z$; $\alpha_{sw} \geq i\varphi_z$	*n/a*
h	*n/a*	$\alpha_{sw} \geq i\varphi_z+\alpha_{en}$ $\alpha_{en} \geq i\varphi_z$; $\alpha_{sw} \geq i\varphi_z$	*n/a*

For every cutting condition a "code" composed by *n* symbols will identify the F_y shape for a multiple fluted endmill. For example, a "IIML" code represents a type II single flute F_y shape characterized by 3 flutes engaged, with the second flute medium overlapping the first and the third one low overlapping the first.

2.3. Surface generating force

Based on the "code" described in the previous section, the shape of F_y in the engagement angle domain is identified according to the cutting parameters and the tool's geometry. The shape of corresponding surface error profile can be foreseen by analysing the shape assumed by the F_y in the interval which the machined surface is generated (i.e surface generating force). Thanks to this, the axial distribution of the surface generating force is obtained (Fig. 2).

2.4. Form error and analytical equations

The method previously described classifies every surface generating force shape by knowing the type of single flute F_y shape, the number of flutes cutting simultaneusly *n* and the degree of overlap between the *n*-1 couple of single flute F_y shapes involved in the cut. In this section, the axial positions for the key points, characterizing every possible surface generating force shape are presented. Depending on the type of single flute F_y shape and the degree of overlap between the first single flute F_y shape and the *i*-th following single flute F_y shape involved in the cut, the analytical expressions of the axial positions for the key points, characterizing the surface generating force shape are reported in Table 2. These equations depend only on the cutting parameters and the tool geometry. Moreover, it must be noted that some of the axial positions produced by the equations, depending on the cutting conditions, may be either negative or higher than *ap*.

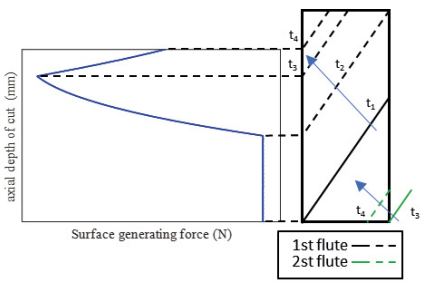

Fig. 2. Example of surface generating force

Table 2. Analytical equations.

	Type I
L	$z_L{}^i = {(i\varphi_z - \alpha_{en})}/{k_b}$
M	$z_M{}^i = {(\alpha_{sw} + i\varphi_z - \alpha_{en})}/{k_b}$
H	$z_M{}^i$
	Type II
	$z_3 = ap - {\alpha_{en}}/{k_b}$
L	$z_L{}^i = {(i\varphi_z - \alpha_{en})}/{k_b}$
M	$z_L{}^i \quad ; \quad z_{Mi} = a_p - {i\varphi_z}/{k_b}$
H	$z_{Hi} = z_3 + {i\varphi_z}/{k_b} \quad ; z_m{}^i = {i\varphi_z}/{k_b}$
m	$z_L{}^i ; \quad z_m{}^i ; \quad z_M{}^i ; \quad z_{2m}{}^i = z_3 - {i\varphi_z}/{k_b} ;$
h	$z_m{}^i ; \quad z_H{}^i ; \quad z_{2m}{}^i$
	Type III
L	$z_L{}^i = {(i\varphi_z - \alpha_{en})}/{k_b} ; \quad z_{2L}{}^i = {(i\varphi_z + \alpha_{sw} - \alpha_{en})}/{k_b}$
M	$z_{2L}{}^i \quad ; \quad z_{max}{}^i = {(i\varphi_z + \alpha_{sw} - \alpha_{enc})}/{k_b}$
H	$z_{2L}{}^i ; \quad z_{max}{}^i$

In such cases, these axial positions must not be considered for the characterization of the surface error because, despite their influence on the shape of the cutting force, they are not involved in the surface generation process. Moreover, in case of Type II, z_M and z_m could not be found in the force profile due to a new cutting flute engagement (M or L subsequent overlap). This aspect should be further investigated.

3. Validation

The effectiveness of the proposed equations has been validated with both numerical simulations and experimental tests. In detail, numerical simulations were used to predict the surface generating force shape exploiting the mechanistic cutting model of equation (5). Instead, experimental tests were used to acquire the surface error shape.

3.1. Setup

Three milling tests were conducted on a a DMG MORI DMU 75 machine using a 12mm diameter four flutedend mill (Garant 202552) with 45° of helix angle. Each test aims at identifying different surface error shapes for the same type II single flute F_y shape, but with different *n* and degrees of overlap. The cutting parameters adopted in each test are summarized in Table 3. These tests were performed on a stiff workpiece (50x80x90mm) made of aluminum (6082-T4). Before each test, the workpiece surface was flattened and measured using an on-board measuring probe (RENISHAW PowerProbe 60). Then cut was performed and the newly generated surface was measured with the same probe. The starting and the machined surfaces were obtained as mean of 5 sets of points acquired along the axial depth of cut with 0.25mm step. The surface error shape was finally obtained as the the difference between the starting and the machined surface, considering the radial depth of cut. As far as surface generating force shape prediction is concerned the required cutting coefficients were *Ktc*=752.9 N/mm^2 and *Krc*=200.5 N/mm^2.

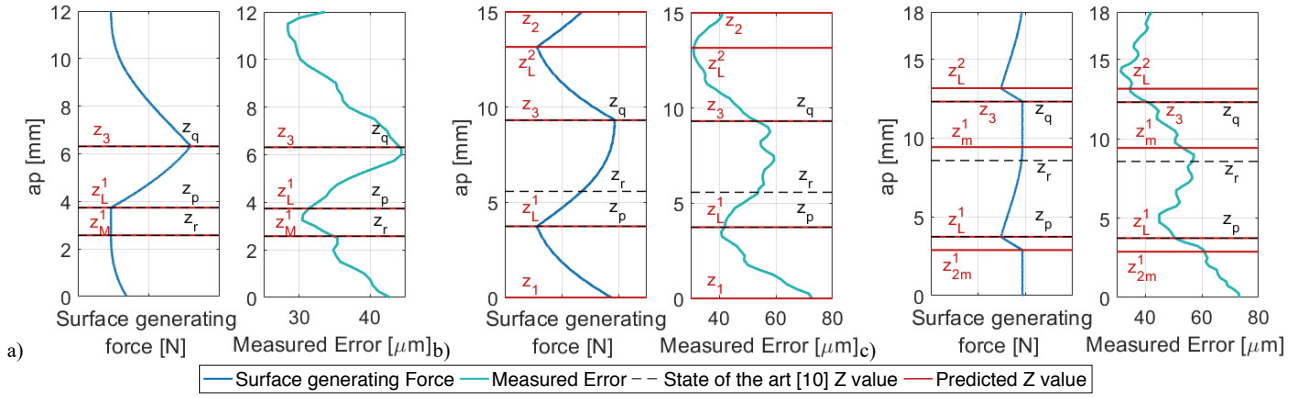

Fig. 3. Predicted force shapes and measured surface error for a) IIM *ap* 12 mm *ar* 2.5 mm b) IIML *ap* 15 mm *ar* 2.5 mm c) IImL *ap* 18 mm *ar* 2.5 mm

Table 3: Milling tests paramters

ar	ap	Force shape code	Spindle speed	Feed per tooth
2.5mm	12mm	IIM	6366 rpm	0.1mm/tooth
2.5mm	15mm	IIML	6366 rpm	0.1mm/tooth
2.5mm	18mm	IImL	6366 rpm	0.1mm/tooth

3.2. Surface error shape and Surface generating force shape

The results obtained are reported in Fig. 3, in which the measured surface error shape are put side by side with the predicted surface generating force shape. In the same figure the results given by the analytical equations (Table 2) of the key points apare reported, together with the results of the analytical equation reported by Desai et al [10]. The three predicted force shapes are in good agreement with the form of the measured error. In detail, with *ap*=12mm (Fig. 3a), the equations proposed identifies the key points of the surface error profile and match the results by Desai et al [10]. As the axial depth of cut increases (*ap*=15mm) and more flutes are involved in the cut (Fig. 3b), the equations by Desai et al [10] fail to represent these key points because this condition of overlap was not considered. The proposed expressions, instead, are still effective in identifying the key points of the surface error profile. Nonentheless, with high values of *ap* (18mm) the impact of variation of the tool stiffness along the axial depth of cut becomes significant (Fig. 3c) and as exptected the surface error profile is twisted, slightly shifting the positions of the key points.

4. Conclusions

In this paper a novel approach to classify the shapes of the cutting forces and the related surface generating forces in 3-axis milling is presented. The analytical equations proposed to predict the key points of surface errors could be useful to ease the surface error prediction and the in-line surface measurements, since they could be exploited to reduce the number of points to be analyzed. Future works will focus on investigating the influence of the overlap on key points suppression as well as testing other categories, different cutting strategies (up milling) and include the impact of the tool/workpiece stiffness to predict the surface error.

Acknowledgments

The authors would like to thank Machine Tool Technology Research Foundation (MTTRF) and its supporters for the loaned machine tool (DMG MORI DMU 75 MonoBlock).

References

[1] X. Zhang, W. Zhang, J. Zhang, B. Pang, and W. Zhao, ‘Systematic study of the prediction methods for machined surface topography and form error during milling process with flat-end cutter’, *Proceedings of the Institution of Mechanical Engineers, Part B: Journal of Engineering Manufacture*, vol. 233, no. 1, pp. 226–242, 2019, doi: 10.1177/0954405417740924.

[2] A. Scippa, N. Grossi, and G. Campatelli, ‘FEM based cutting velocity selection for thin walled part machining’, *Procedia CIRP*, 2014.

[3] S. Wimmer and M. Zaeh, ‘The Prediction of Surface Error Characteristics in the Peripheral Milling of Thin-Walled Structures’, *Journal of Manufacturing and Materials Processing*, vol. 2, no. 1, p. 13, 2018, doi: 10.3390/jmmp2010013.

[4] N. Grossi, A. Scippa, L. Croppi, L. Morelli, and G. Campatelli, ‘Adaptive toolpath for 3-axis milling of thin walled parts’, *MM Science Journal*, vol. 2019, no. November, pp. 3378–3385, 2019, doi: 10.17973/MMSJ.2019_11_2019096.

[5] I. Nishida, R. Okumura, R. Sato, and K. Shirase, ‘Cutting force and finish surface simulation of end milling operation in consideration of static tool deflection by using voxel model’, *Procedia CIRP*, vol. 77, no. Hpc, pp. 574–577, 2018, doi: 10.1016/j.procir.2018.08.218.

[6] T. L. Schmitz and B. P. Mann, ‘Closed-form solutions for surface location error in milling’, *International Journal of Machine Tools and Manufacture*, vol. 46, no. 12–13, pp. 1369–1377, Oct. 2006, doi: 10.1016/j.ijmachtools.2005.10.007.

[7] W. S. Yun, J. H. Ko, D. W. Cho, and K. F. Ehmann, ‘Development of a virtual machining system, Part 2: Prediction and analysis of a machined surface error’, *International Journal of Machine Tools and Manufacture*, vol. 42, no. 15, pp. 1607–1615, 2002, doi: 10.1016/S0890-6955(02)00138-4.

[8] M. N. Islam, H. U. Lee, and D. W. Cho, ‘Prediction and analysis of size tolerances achievable in peripheral end milling’, *International Journal of Advanced Manufacturing Technology*, vol. 39, no. 1–2, pp. 129–141, 2008, doi: 10.1007/s00170-007-1188-4.

[9] L. Yang, R. E. DeVor, and S. G. Kapoor, ‘Analysis of force shape characteristics and detection of depth-of-cut variations in end milling’, *Journal of Manufacturing Science and Engineering, Transactions of the ASME*, vol. 127, no. 3, pp. 454–462, 2005, doi: 10.1115/1.1947207.

[10] K. A. Desai and P. V. M. Rao, ‘On cutter deflection surface errors in peripheral milling’, *Journal of Materials Processing Technology*, vol. 212, no. 11, pp. 2443–2454, Nov. 2012, doi: 10.1016/J.JMATPROTEC.2012.07.003.